Inverse Geometrico-Static Problem of Cable-Network-Driven Parallel Robots

Edoardo Ida'

Abstract Cable-Driven Parallel Robots (*CDPRs*) can achieve large workspaces since long cables can be spooled on winches. However, the end-effector (*EE*) is typically surrounded by multiple cables that must remain in tension and may interfere with each other or with the environment, thereby limiting practical applicability. This paper proposes a novel class of *CDPRs* in which cables are routed through a network of intermediate points, referred to as cable-network-driven parallel robots. In this paper, a redundantly actuated *CDPR* with an underconstrained *EE* is shown posessing a large workspaces even in the presence of obstacles. Topological, modeling, and inverse problem challenges are discussed.

1 Introduction

Cable-Driven Parallel Robots (*CDPRs*) move their end-effector (*EE*) by spooling cables routed through frame-fixed pulleys and attached to the *EE* [1]. A distinctive feature of *CDPRs* is their ability to achieve exceptionally large workspaces [2]. However, their industrial adoption remains limited due to two fundamental constraints: (i) the unilateral tensile nature of cable actuation, and (ii) the resulting need to surround the *EE* with multiple tensioned cables. In practical applications, cable interference with other cables and the environment must be limited, and cables must remain outside the task space. Overconstrained *CDPRs*, with more cables than the degrees of freedom (*DoFs*) of the *EE*, increase wrench capability by surrounding the *EE* with cables but are effective mainly in limited scenarios, such as motion simulation or planar tasks where operation occurs outside the plane

Edoardo Ida'
Dept. of Industrial Engineering, University of Bologna, 40136 Bologna, Italy
e-mail: edoardo.ida2@unibo.it

of motion [3]. Suspended architectures route cables from elevated positions, keeping them largely outside the task space but reducing wrench-generation capability. Overconstrained suspended systems [4] suit constant-orientation tasks, where interference can be mitigated through geometric optimization, whereas underconstrained architectures achieve high speed and acceleration in horizontal motion tracking [5] but provide limited dexterity.

CDPRs that route cables from the frame to the *EE* are inherently limited in dexterity and workspace accessibility. To address these limitations, nonconventional architectures have been explored. Some exploit kinematic redundancy [8] by enlarging or adapting the workspace through actuation means other than cables, such as linear sliders [7] or drones [6] that reposition cable exit points. However, non-cable actuators introduce intrinsic limitations, including limited payload for aerial robots and restricted stroke or mobility for linear sliders. Others rely on advanced cable routing strategies [9], environmental interactions to deflect cables [10], or articulated *EE* designs [11]. While promising, particularly for planar systems [9] or highly structured environments [10, 11], these solutions do not readily scale to 6-*DoF* robots operating in unstructured environments.

This paper introduces an architecture in which cables are routed through, or attached to, a network of intermediate points (nodes), with only a subset directly connected to the *EE*, which is therefore underconstrained [12]. Some cables act on the *EE*, while others pull on each other, enabling continuous node reconfiguration and displacement of cables from the task space. This concept was first hinted at in [13], where cables pull on one another to modify tension orientation. Here, the concept is extended by analyzing the network properties of actuation and routing, leading to the definition of cable-network-driven parallel robots (*CNDPRs*). The paper studies the inverse geometrico-static model of planar *CNDPRs* through two representative examples, each driving an underconstrained 3-*DoF* planar *EE* with four cables. It is shown that the considered *CNDPRs* are redundantly actuated despite having an underconstrained *EE*. An algorithm is proposed to compute solution sets with obstacle-avoidance capabilities, and demonstrated through a path-planning example. The paper is organized as follows: Sec. 2 presents the system model, Sec. 3 formulates the inverse problem, Sec. 4 illustrates the solution and system capabilities via path planning, and Sec. 5 concludes the paper.

2 Modeling Overview

This section introduces the model of a planar *CNDPR*. Oxy is a fixed frame, while $Px'y'$ is attached to the *EE* reference point and center of mass P. The position of P is given by the vector $\mathbf{p}$ (planar distance vectors belong to $\mathbb{R}^2$), and the rotation matrix $\mathbf{R}(\theta) \in \mathbb{R}^{2\times 2}$ defines the orientation of $Px'y'$. The *EE* pose is thus $\boldsymbol{\zeta} = [\mathbf{p}^T, \theta]^T$. The *CNDPRs* of this paper consist of (Fig. 1):

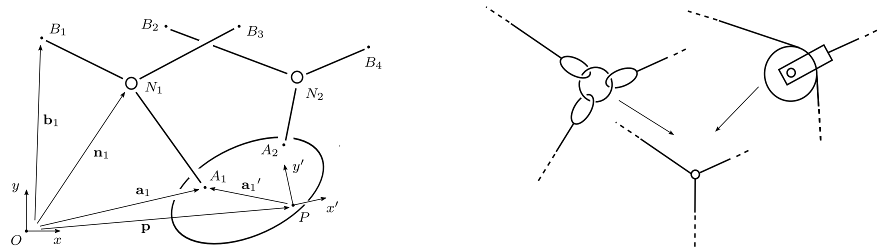

Fig. 1: Overview of the *CNDPR* on the left, nodes model on the right

- $n_f = 4$ frame anchor points B_i, with $i = 1, \ldots, n_f$, described by constant vectors $\mathbf{b}_i$; cables enter the workspace exclusively through these points.
- $n_n = 2$ intermediate routing points (nodes) N_i, with $i = 1, \ldots, n_n$, described by variable vectors $\mathbf{n}_i$. As introduced in Sec. 1 and shown in Fig. **??**, cables may be attached to or pass through these nodes (both cases are referred to as being *connected to* the node).
- $n_e = 2$ *EE* anchor points A_i, with $i = 1, \ldots, n_e$, described by $\mathbf{a}_i = \mathbf{p} + \mathbf{R}\mathbf{a}_i'$, where $\mathbf{a}_i'$ is constant in $Px'y'$; cables are only attached to these points.

For simplicity, cables are modeled as massless straight lines, and nodes are assumed massless and infinitesimal. In practice, nodes could be realized as rings or pulley systems, as illustrated in Fig. 1. A system of this type is geometrically fully defined by the node positions (four scalar variables in this case) and the *EE* pose (three scalar variables). Depending on the number of actuated cables and the chosen routing topology through anchors and nodes the computation of actuated cable lengths varies. In general, determining the node positions (and consequently the cable lengths) given the *EE* pose is referred to as the *Inverse Problem*, whereas determining the *EE* pose (with node positions as intermediate variables) given the cable lengths is referred to as the *Direct* or *Forward Problem*.

Consider a simple network in which two pairs of cables, each exiting a frame anchor, are *connected to* two nodes, as shown in Fig. 1. We define a vector for each *branch* of the cable network, corresponding to each segment connecting an anchor to a node:

$$\mathbf{t}_{11} = \mathbf{n}_1 - \mathbf{b}_1, \qquad \mathbf{t}_{13} = \mathbf{n}_1 - \mathbf{b}_3, \qquad \mathbf{t}_{22} = \mathbf{n}_2 - \mathbf{b}_2, \qquad \mathbf{t}_{24} = \mathbf{n}_2 - \mathbf{b}_4 \quad (1)$$

$$\mathbf{t}_1 = \mathbf{a}_1 - \mathbf{n}_1, \qquad \mathbf{t}_2 = \mathbf{a}_2 - \mathbf{b}_2 \quad (2)$$

With n_f independently actuated cables, the same network may correspond to different *CNDPRs*, depending on whether cables are routed through or attached to the nodes. Two routing examples are therefore introduced in Fig. 2. In the first case (Fig. 2 on the left), the actuated cables exiting from B_1

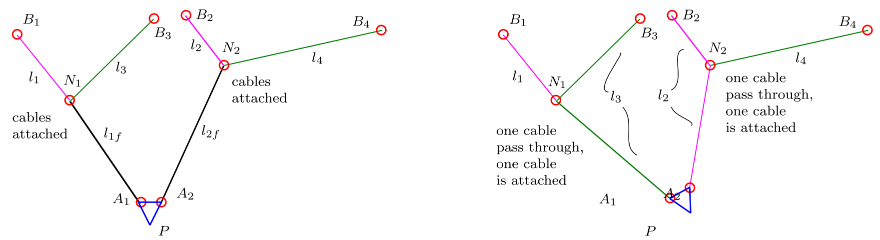

Fig. 2: Distinct cable routings characterized by the same network. Red dots are anchors or nodes, blue lines represent the *EE*, black lines are fixed-lenght cables, actuated cables are represented in green and magenta.

and B_3 are *attached to* N_1, while those exiting from B_2 and B_4 are *attached to* N_2. Their variable lengths are given by:

$$l_1 = \|\mathbf{t}_{11}\|, \qquad l_2 = \|\mathbf{t}_{22}\|, \qquad l_3 = \|\mathbf{t}_{13}\|, \qquad l_4 = \|\mathbf{t}_{24}\| \tag{3}$$

Two non-actuated cables of lengths l_{1f} and l_{2f} connect N_1 to A_1 and N_2 to A_2, respectively. The resulting system resembles a planar aerial cable-towed system, in which two drones replace the actuated cables to position N_1 and N_2. Despite employing four cables, the inverse problem remains underdetermined, as infinitely many node configurations can yield the same *EE* pose. In the second case (Fig. 2 on the right), the actuated cables exiting from B_1 and B_4 are *attached to* N_1 and N_2, respectively, while the cables exiting B_2 and B_3 are routed through N_2 and N_1 and attached to A_2 and A_1, respectively. The inverse problem remains underdetermined, and the actuated cable lengths are:

$$l_1 = \|\mathbf{t}_{11}\|, \qquad l_2 = \|\mathbf{t}_{22}\| + \|\mathbf{t}_2\|, \qquad l_3 = \|\mathbf{t}_{13}\| + \|\mathbf{t}_3\|, \qquad l_4 = \|\mathbf{t}_{24}\| \tag{4}$$

Consider the statics of all moving elements for the given network, namely the *EE* and the nodes, independently of the routing scheme. Let τ_{11}, τ_{13}, τ_{22}, τ_{24}, τ_1, and τ_2 denote the tensile forces in the branches $\hat{\mathbf{t}}_{11}, \ldots, \hat{\mathbf{t}}_2$ defined in Eqs. (1) and (2), where $\hat{\cdot}$ denotes a unit vector. Static equilibrium at the nodes yields:

$$\hat{\mathbf{t}}_{11}\tau_{11} + \hat{\mathbf{t}}_{13}\tau_{13} = \hat{\mathbf{t}}_1\tau_1, \qquad \hat{\mathbf{t}}_{22}\tau_{22} + \hat{\mathbf{t}}_{24}\tau_{24} = \hat{\mathbf{t}}_2\tau_2 \tag{5}$$

and if $\tilde{\cdot}$ is the matrix representation of the vector product, m the *EE* mass, and $\mathbf{g}$ the gravitational acceleration, the statics of the *EE* is:

$$\hat{\mathbf{t}}_1\tau_1 + \hat{\mathbf{t}}_2\tau_2 = m\mathbf{g}, \qquad \tilde{\mathbf{t}}_1\mathbf{R}\mathbf{a}'_1\tau_1 + \tilde{\mathbf{t}}_2\mathbf{R}\mathbf{a}'_2\tau_2 = 0 \tag{6}$$

Equations (5) and (6) can be summarized in the following system of 7 equations:

$$\begin{bmatrix} -\hat{\mathbf{t}}_1 & \hat{\mathbf{t}}_{11} & \hat{\mathbf{t}}_{13} & \mathbf{0}_{2\times1} & \mathbf{0}_{2\times1} & \mathbf{0}_{2\times1} \\ \mathbf{0}_{2\times1} & \mathbf{0}_{2\times1} & \mathbf{0}_{2\times1} & -\hat{\mathbf{t}}_2 & \hat{\mathbf{t}}_{22} & \hat{\mathbf{t}}_{24} \\ \hat{\mathbf{t}}_1 & \mathbf{0}_{2\times1} & \mathbf{0}_{2\times1} & \hat{\mathbf{t}}_2 & \mathbf{0}_{2\times1} & \mathbf{0}_{2\times1} \\ \tilde{\mathbf{t}}_1\mathbf{R}\mathbf{a}'_1 & 0 & 0 & \tilde{\mathbf{t}}_2\mathbf{R}\mathbf{a}'_2 & 0 & 0 \end{bmatrix} \begin{bmatrix} \tau_1 \\ \tau_{11} \\ \tau_{13} \\ \tau_2 \\ \tau_{22} \\ \tau_{24} \end{bmatrix} = \begin{bmatrix} \mathbf{0}_{4\times1} \\ m\mathbf{g} \\ 0 \end{bmatrix} \Rightarrow \boldsymbol{\Xi}\boldsymbol{\tau} = \mathbf{w} \qquad (7)$$

3 Inverse Geometrico-Static Problem

If the geometry were assigned, i.e. for a given $\boldsymbol{\Xi}$, the inverse static problem, namely computing the branch tensions $\boldsymbol{\tau}$ from Eq. (7), is generally overdetermined (7 equations, 6 unknowns). Hence, the inverse geometric and inverse static problems cannot, in general, be solved independently. If geometry is not prescribed, the inverse static problem becomes solvable and the overall inverse geometrico-static problem is underdetermined. Indeed, Eq. (7) provides 7 equations in 10 unknowns: the four node coordinates, collected in $\boldsymbol{\nu} = [\mathbf{n}_1^T, \mathbf{n}_2^T]^T$, and the six branch tensions in $\boldsymbol{\tau}$. The resulting solution set is, in general, infinite and has dimension 3. Imposing a specific cable routing further constrains the problem and reduces the solution dimension. The routing of the first example (Fig. 2 on the left) requires enforcing two additional constraints:

$$\|\mathbf{t}_1\| = l_{1f}, \qquad \|\mathbf{t}_2\| = l_{2f} \qquad (8)$$

The routing of the second example (Fig. 2 on the right), neglecting friction at the node and enforcing moment equilibrium about the node, requires instead:

$$\tau_1 = \tau_{11}, \qquad \tau_2 = \tau_{24} \qquad (9)$$

The inverse geometrico-static problem results in 9 Eqs. in 10 unknowns and is characterized by an infinite solution set of dimension 1. The proposed *CNDPR* is therefore redundantly actuated [8], as infinite inverse geometrico-static solutions exist, each corresponding to a different internal geometry and cable tensions.

The solution procedure for the inverse geometrico-static problem is detailed next. Since the solution set is generally infinite and its full characterization is beyond the scope of this paper, a gradient-based nonlinear constrained optimization problem is formulated and commercial solvers are used to compute a single solution near a given initial guess. In path-planning applications, where the input pose varies continuously (Sec. 4), solution continuity is also required. Accordingly, the solution at the previous pose is used as the initial guess, and the variation of inter-node distances between consecutive poses is chosen as the optimization cost. While the former is standard in numerical tracking schemes, the latter is an original proposition for *CNDPRs*, and minimizes *node motion*.

The inverse-problem solutions must yield positive cable tensions. Since Eq. (7) is linear in $\boldsymbol{\tau}$, this array can be computed as an intermediate step, and not treated as problem variables. to this end, Eq. (7) is partitioned as:

$$\boldsymbol{\Xi}_f(\boldsymbol{\nu})\boldsymbol{\tau} = \mathbf{w}_f, \qquad \tilde{\mathbf{t}}_1(\boldsymbol{\nu})\mathbf{R}\mathbf{a}'_1\tau_1 + \tilde{\mathbf{t}}_2(\boldsymbol{\nu})\mathbf{R}\mathbf{a}'_2\tau_2 = 0 \tag{10}$$

where $\boldsymbol{\Xi}_f \in \mathbb{R}^{6\times 6}$ and $\mathbf{w} \in \mathbb{R}^{6\times 1}$ are formed by the first six rows of $\boldsymbol{\Xi}$ and $\mathbf{w}$, respectively, with the explicit dependence on $\boldsymbol{\nu}$ highlighted. The left-hand part of Eq. (10) is used to compute cable tensions when $\boldsymbol{\nu}$ is assigned, a fact which is conventional in most gradient-based numerical solvers. The right-hand part is instead referred to as the *static constraint* [12] and must be satisfied at the solution. The constraints in (8) or (9) can be rearranged in implicit form as:

$$\mathbf{c}(\boldsymbol{\nu}, \boldsymbol{\tau}) = \mathbf{0}_{2\times 1} \tag{11}$$

Finally, let $\mathbf{d}(\boldsymbol{\nu}) = |\mathbf{n}_2 - \mathbf{n}_1|$ denote the distance between the nodes, $\boldsymbol{\nu}_n$ the node configuration at a neighbouring pose, and $\underline{\boldsymbol{\nu}}$, $\overline{\boldsymbol{\nu}}$ the lower and upper bounds on node positions. The optimization problem is then formulated as:

$$\begin{aligned} \min_{\boldsymbol{\nu}} \; & |\mathbf{d}(\boldsymbol{\nu}) - \mathbf{d}(\boldsymbol{\nu}_n)| \\ \text{s.t.} \; & \tilde{\mathbf{t}}_1(\boldsymbol{\nu})\mathbf{R}\mathbf{a}'_1\tau_1 + \tilde{\mathbf{t}}_2(\boldsymbol{\nu})\mathbf{R}\mathbf{a}'_2\tau_2 = 0, \\ & \mathbf{c}(\boldsymbol{\nu}, \boldsymbol{\tau}) = \mathbf{0}_{2\times 1}, \\ & \boldsymbol{\tau} = \boldsymbol{\Xi}_f^{-1}(\boldsymbol{\nu})\mathbf{w}_f \geq \mathbf{0}_{6\times 1}, \\ & \underline{\boldsymbol{\nu}} \leq \boldsymbol{\nu} \leq \overline{\boldsymbol{\nu}} \end{aligned} \tag{12}$$

Equation (12) can be solved, for example, using MATLABs *fmincon* with an *interior-point* algorithm and a *conjugate-gradient* sub-algorithm to accelerate constraint satisfaction. Only an initial guess for the node positions, such as $\boldsymbol{\nu}_n$, is required in addition to the desired *EE* pose, since cable tensions are computed as an intermediate step and used as a constraint as highlighed in Eq. (12).

4 Illustrative Example: Quasi-Static Path Planning

To demonstrate the capabilities of the proposed *CNDPR*, a quasi-static path-planning example is presented. Consecutive static equilibrium configurations are computed, consistent with motion at negligible speeds and accelerations. The second routing example is considered (Fig. 2 on the right); the geometric parameters are reported in Tab. 1, and $\mathbf{c}(\boldsymbol{\nu}, \boldsymbol{\tau})$ in Eq. (12) is defined as:

$$\mathbf{c}(\boldsymbol{\nu}, \boldsymbol{\tau}) = \begin{bmatrix} \tau_1 - \tau_{11} \\ \tau_2 - \tau_{24} \end{bmatrix} = \mathbf{0}_{2\times 1} \tag{13}$$

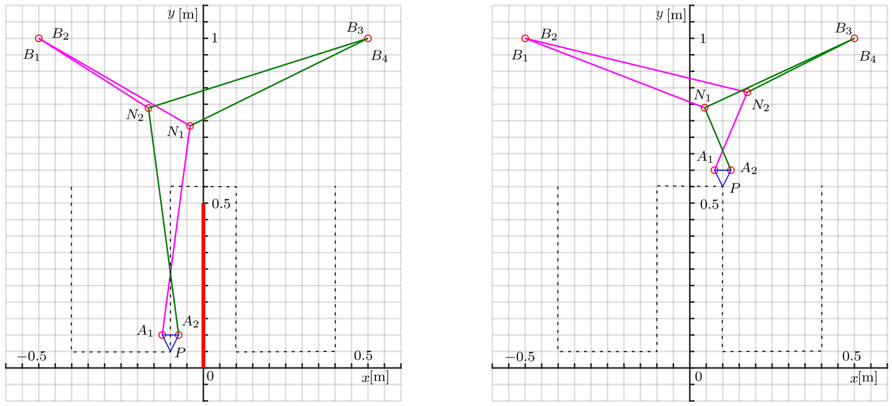

Fig. 3: The *CNDPR* in two configurations. On the left $\mathbf{p} = \mathbf{p}_{w,3}$ and on the right $\mathbf{p} = \mathbf{p}_{w,5}$. Red circles are anchors or nodes, blue lines form the *EE*, the red line is the obstacle, actuated cables are in green and magenta. The path is dashed.

i	1	2	3	4	i	1	2	i	1	2
$\mathbf{b}_i$ [m]	$\begin{bmatrix}-0.5\\1\end{bmatrix}$	$\begin{bmatrix}-0.5\\1\end{bmatrix}$	$\begin{bmatrix}0.5\\1\end{bmatrix}$	$\begin{bmatrix}0.5\\1\end{bmatrix}$	$\mathbf{n}_{i0}$ [m]	$\begin{bmatrix}-0.5\\1\end{bmatrix}$	$\begin{bmatrix}-0.5\\1\end{bmatrix}$	$\mathbf{a}'_i$ [m]	$\begin{bmatrix}-0.025\\0.05\end{bmatrix}$	$\begin{bmatrix}0.025\\0.05\end{bmatrix}$

Table 1: Geometrical parameters of the *CNDPR*

i	1	2	3	4	5	6	7	8
$\mathbf{p}_{w,i}$ [m]	$\begin{bmatrix}-0.4\\0.55\end{bmatrix}$	$\begin{bmatrix}-0.4\\0.05\end{bmatrix}$	$\begin{bmatrix}-0.1\\0.05\end{bmatrix}$	$\begin{bmatrix}-0.1\\0.55\end{bmatrix}$	$\begin{bmatrix}0.1\\0.55\end{bmatrix}$	$\begin{bmatrix}0.1\\0.05\end{bmatrix}$	$\begin{bmatrix}0.4\\0.05\end{bmatrix}$	$\begin{bmatrix}0.4\\0.55\end{bmatrix}$

Table 2: Path waypoints

	between $\mathbf{p}_{w,1}$ and $\mathbf{p}_{w,4}$	between $\mathbf{p}_{w,4}$ and $\mathbf{p}_{w,5}$	between $\mathbf{p}_{w,5}$ and $\mathbf{p}_{w,8}$
$\underline{n}_{1,x} = \underline{n}_{2,x}$ [m]	-0.5	$-0.5 + 0.5(p_x + 0.1)/0.2$	0
$\overline{n}_{1,x} = \overline{n}_{2,x}$ [m]	0	$+0.5(p_x + 0.1)/0.2$	0.5

Table 3: Bounds on x components of $\boldsymbol{\nu}$, p_x is the same component of $\mathbf{p}$

The planned path consists of straight-line segments connecting the waypoints $P_{w,i}$, defined by their positions $\mathbf{p}_{w,i}$, with $i = 1, \ldots, 8$ (Tab. 2). The path circumvents an obstacle represented by the line segment connecting $[0, 0]^T$ m and $[0, 0.5]^T$ m (Fig. 3). Obstacle avoidance is achieved by appropriately selecting the solution bounds $\underline{\boldsymbol{\nu}} \leq \boldsymbol{\nu} \leq \overline{\boldsymbol{\nu}}$ in Eq. (12). Since the solution set is infinite, these bounds restrict the solver to geometrically feasible, obstacle-avoiding configurations. Three sets of bounds are considered,

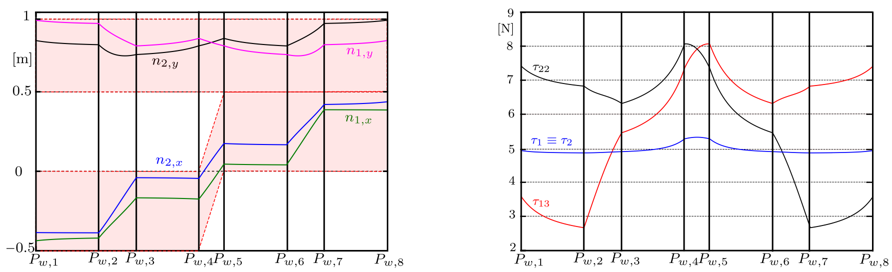

Fig. 4: Path planning results. On the left the node coordinates are shown (red dashed area denotes coordinates limits), and on the right cable tensions are shown. Bold vertical lines denotes the passage through a waypoint.

one of which explicitly depends on $\mathbf{p}$ and enables obstacle circumvention with continuous node configurations. The bounds on the y components are fixed to $\underline{n}_{1,y} = \underline{n}_{2,y} = 0.5\,\text{m}$ and $\overline{n}_{1,y} = \overline{n}_{2,y} = 0.95\,\text{m}$, while the bounds on the x components are reported in Tab. 3. The initial guess for solving (12) at $\mathbf{p} = \mathbf{p}_{w,1}$ is $\boldsymbol{\nu}_n = [\mathbf{n}_{10}^T, \mathbf{n}_{20}^T]$ (Tab. 1). Figure 4 shows the evolution of the nodes coordinates while following the assigned trajectory, respecting the prescribed bounds, and keeping all cables under tension while circumventing the obstacle.

5 Conclusions

This paper introduced cable-network-driven parallel robots (*CNDPRs*). Using an introductory planar architecture, it highlighted their topological properties and showed their redundantly actuated yet underconstrained structure. Their inverse geometrico-static problem was formulated as a constrained optimization, with a cost function designed to promote solution continuity. Its solution was used to demonstrate a path-planning example, showing that the *CNDPR* can be fully controlled while keeping cable under tension and avoiding workspace obstacles. This preliminary investigation is only a preliminary analysis on the potential of *CNDPRs*, as increasing the number of cables, exploring alternative network topologies, and adopting different routing strategies open up a wide range of scenarios and applications.

Acknowledgements I would like to express my gratitude to Prof. Marco Carricato, Dr. Jean-Pierre Merlet, and Dr. Marc Gouttefarde for insightful discussions on the topic.

References

1. Ida E., Mattioni, V.: Cable-Driven Parallel Robot Actuators: State of the Art and Novel Servo-Winch Concept. Actuators, vol. 11(10), paper no. 290, pp. 1-13, 2022, doi: 10.3390/act11100290.
2. Su Y., Qiu, Y., Liu, P., Tian, J., Wang, Q., Wang X.: "Dynamic modeling, workspace analysis and multi-objective structural optimization of the large-span high-speed cable-driven parallel camera robot". Machines, vol. 10(7), paper no. 565, pp. 1-31, 2022, doi: 10.3390/machines10070565.
3. Iturralde K., Feucht, M., Rongbo, H., Pan, W., Schlandt, M., Linner, T., ..., Elia, L. "A cable driven parallel robot with a modular end effector for the installation of curtain wall modules". In: Proceedings of the 37th ISARC, IARCC, pp. 1472-1479, Kitakyushu, Japan 27-29 Oct. 2020, doi: 10.22260/ISARC2020/0204.
4. Izard J.-B., Dubor, A., Hervé, P. E., Cabay, E., Culla, D., Rodriguez, M., Barrado M.: "Large-scale 3D printing with cable-driven parallel robots". Construction Robotics vol. 1, pp. 6976, 2017, doi: 10.1007/s41693-017-0008-0.
5. Angelini M., Ida, E., Bertin, D., Mantovani, E., Bazzi, D., Orassi, V., Carricato, M.: "An underactuated cable-driven parallel robot for marine automated launch and recovery operations". Journal of Mechanisms and Robotics, vol. 17(1), paper no. 010906, pp. 1-10, 2025, doi: 10.1115/1.4065394.
6. De Carli N., Belletti, R., Buzzurro, E., Testa, A., Notarstefano, G., Tognon M.: "Distributed NMPC for Cooperative Aerial Manipulation of Cable-Suspended Loads," IEEE Robotics and Automation Letters, vol. 10, paper no. 10, pp. 10546-10553, doi: 10.1109/LRA.2025.3604703.
7. Trautwein F., Dietrich D., Pott A., Verl A.: "Strategy for Topological Reconfiguration of Cable-Driven Parallel Robots". Journal of Mechanisms and Robotics, vol. 17(1), paper no. 010908, pp. 1-10, 2025 10.1115/1.4065642.
8. Merlet J.-P.: "On the Redundancy of Cable-Driven Parallel Robots". In: P. Flores e F. Viadero (eds.), New Trends in Mechanism and Machine Science, Springer, pp. 3139, 2015, doi: 10.1007/978-3-319-09411-3_4.
9. Behroozi F., Mersi, R., Benoist, A., Ying Yong, R., Cardou, P., Caro S.: "A Three-Actuator Cable-Driven Parallel Robot With a Rectangular Workspace". Journnal of Mechanisms and Robotics, vol. 17(1), paper no. 010905, pp. 1-8, 2025, doi: 10.1115/1.4065393.
10. Rushton M., Khajepour A.: "An Atlas-Based Approach to Planar Variable-Structure Cable-Driven Parallel Robot Configuration-Space Representation". IEEE Transactions on Robotics, vol 39(2), pp. 15941606. 2023, doi: 10.1109/TRO.2022.3218996.
11. Rasheed T., Long P., Padir T., Caro S.: "Wrench Capability Analysis of a Planar Dual-Platform Cable-Driven Parallel Robot". In: Proceedings of the ASME 2023 International Design Engineering Technical Conferences and Computers and Information in Engineering Conference vol. 8: 47th Mechanisms and Robotics Conference (MR), Boston, Massachusetts, USA, 20-23 August 2023, doi: 10.1115/DETC2023-116412.
12. Ida E., Carricato M.: Static workspace computation for underactuated cable-driven parallel robots. Mechanism and Machine Theory, vol. 193, paper no. 105551, pp. 1-19, 2024, doi: 10.1016/j.mechmachtheory.2023.105551
13. Merlet, J.-P.: "Managing the redundancy of $N-1$ wire-driven parallel robots". In: Lenarcic J., Husty M. (eds.), Latest Advances in Robot Kinematics, Springer, pp. 405-412, 2012, doi: 10.1007/978-94-007-4620-6_51.